



Degradation enhancement of methylene blue on ZnO nanocombs synthesized by thermal evaporation technique

M. Rashad^{a,b}, N.M. Shaalan^{a,*}, Alaa M. Abd-Elnaiem^a

^aNano and Functional Materials Laboratory, Faculty of Science, Physics Department, Assiut University, Assiut 71516, Egypt, Tel. +20 882412229; Fax: +20 882342708; emails: mohamed.ahmed24@science.au.edu.eg (M. Rashad), nshaalan@aun.edu.eg (N.M. Shaalan), alaa.abd-elnaiem@science.au.edu.eg (A.M. Abd-Elnaiem)

^bFaculty Science, Department of Physics, University of Tabuk, P.O. Box 741, Tabuk 71491, Saudi Arabia

Received 14 July 2015; Accepted 3 March 2016

ABSTRACT

Different zinc oxide (ZnO) morphologies were synthesized via a thermal evaporation-like technique without a catalyst introduction. The morphology of ZnO has been controlled by varying the evaporation pressure of ambient air. X-ray diffractometer and field emission scanning electron microscope were used for crystallinity and morphology investigation, respectively. The X-ray data confirmed the purity and crystallinity of the as-prepared ZnO structure. A variation of the pressure led to different morphologies of ZnO nanostructure such as nanocombs and nanorods. The influence of these different morphologies on the photocatalytic activity was performed on a water wasted methylene blue. The results showed the geometry of one-dimensional nanostructures deposited at different pressures strongly controls the photocatalytic activity of ZnO. The most suitable photocatalytic performance was recorded for ZnO deposited at 0.15 Torr, which showed one-side nanocombs of long nails.

Keywords: Nanostructures; ZnO; Thermal evaporation; Photocatalytic

1. Introduction

Recently, researchers have paid attention to obtain various structures of materials in nanoscale, looking for new or enhanced properties of these materials. Nanostructured materials have drawn considerable interest because of their special properties such as surface-to-volume ratio, high activity, special electronic properties, and unique optical properties. Wide band gap semiconductors have a great attention due to their wide applications. They express novel physical and chemical properties associated with their low

dimensionality and size confinement [1]. The properties and performance of oxide-based devices can be dramatically influenced by their morphology [2,3]. A considerable dissimilarity for the geometry of one-dimensional (1D) nanostructure can be observed in many prepared materials, depending on the preparation methods. It is known that when nanoparticulate materials are used the average crystallite size is considered, while when 1D material is used the specific geometry of every crystal is considered. Thus, creative kinds of 1D nanomaterial have recently been successfully targeted [4–6]. Among these materials, there is a much interest of metal oxide, especially zinc oxide (ZnO). ZnO is the most promising *n*-type materials

*Corresponding author.

and exhibits both semiconducting and piezoelectric properties [7]. ZnO thin films have a wide band gap of 3.37 eV and an exciton binding energy of 60 meV. Accordingly, ZnO has been used as photocatalyst for water purification [8], UV light-emitting diodes [9,10], field emission devices [11], solar cells [4,12], and gas sensors [13].

Several chemical and physical methods can be used to prepare ZnO nanostructures, such as electrochemical deposition [14], sol-gel [15], chemical vapor deposition [16], spray pyrolysis [17], thermal evaporation [18], ultrasonic irradiation [19], sputtering [20], and hydrothermal process [21]. Among these methods, the thermal evaporation method has been widely used due to low cost, simplicity, and utilization for controlling the morphology.

The photocatalytic process-based semiconducting oxides have been received significant attention as environment-friendly, low production cost, and sustainable treatment technology in the water purification [22,23]. The ability of advanced oxidation technology has been widely established to remove persistent organic compounds and micro-organisms in water [24,25]. According to the simplified Langmuir-Hinshelwood kinetic model, the reaction occurs on the surface of a photocatalytic layer. Therefore, any increase in the active surface area or changes the structure geometry of the oxide would optimize the oxide performance.

Controlling the morphology of synthesis ZnO is very important to nanoscale science. The morphology of ZnO nanostructures can be controlled via different techniques [5–9]. The synthesizing parameters during the thermal evaporation process, such as temperature and pressure, have an important influence on the structure and morphology of the product [26]. Therefore, we report on the formation of various morphologies of ZnO nanostructures by one-step thermal evaporation-like technique without the presence of a catalyst at relatively low deposition pressures. Another main goal of this study is to investigate the effects of pressure on the structural parameters and morphology and to correlate the morphology of ZnO nanostructures and their photocatalytic performance demonstrated.

2. Experimental techniques

The fabrication of ZnO was carried out using the thermal evaporation method, following the procedure discussed elsewhere [2,27]. The commercial ZnO powder (purity 99.99% from Sigma-Aldrich) of 10 mg was placed in a small alumina crucible which was covered by SiO₂/Si substrate. The chamber was evacuated

using a rotary vacuum pump up to deposition pressures of 0.15, 0.3, 0.7, and 1 Torr of ambient air. The crucible was then heated from room temperature (RT) to 900°C within three minutes and maintained at this temperature for one hour. At the end of the deposition, the crucible was cooled down to RT under the same pressure, leading to a substrate surface coated with a thick layer of ZnO products.

The surface morphologies of ZnO nanostructures were characterized by field emission scanning electron microscopy (FE-SEM) Model JEOL, FE-SEM 6700 operating at 5 kV. The crystalline structures of the ZnO samples were characterized by X-ray diffraction (XRD) using a diffractometer with CuK_α radiation Model Shimadzu XRD-6100. The XRD charts were measured within a range of 20°–65° at a scanning rate of 2°/min.

The UV-vis absorbance spectra were measured using Lambda 750 UV-vis spectrophotometer with a scanning rate of 5 nm/s. The photocatalytic activity of ZnO was estimated by the degradation of methylene blue (MB) of 1 × 10⁻⁶ M. The experiment was carried out in a Pyrex reactor and an artificial sunlight simulator of 100 mW/cm² Model Oriel SO12A Solar Simulators associated with an ultraviolet filter. The degradation of MB in water was determined by monitoring the changes of the main absorbance peak observed at a wavelength of 664 nm. The photocatalytic efficiency (η) of MB has been evaluated by using Eq. (1):

$$\eta (\%) = \frac{C_0 - C_t}{C_0} \times 100 \quad (1)$$

where C_0 is the initial dye concentration and C_t the residual dye concentration after the irradiation time (t).

3. Results and discussions

3.1. Crystal structure and morphology of ZnO nanostructures

Fig. 1 shows the XRD patterns of ZnO deposited on Si substrate at various deposition pressures of 0.15, 0.3, 0.7, and 1.0 Torr, corresponding to sample I, II, III, and IV, respectively. It can be seen that the observed peaks are in good agreement with a hexagonal structure of ZnO ($a = 3.248 \text{ \AA}$ and $c = 5.199 \text{ \AA}$), and consistent with the standard values of pure ZnO crystal (JCPDS Card No. 36-1451). Clear and sharp diffractions revealed the high crystallinity of the deposited ZnO films. The diffractions of ZnO films observed at 32°, 34.4°, 36.3°, 47.7°, 56.7°, and 62.9° are corresponding to the planes of (1 0 0), (0 0 2), (1 0 1), (1 0 2), (1 1 0), and (1 0 3), respectively. Additionally, no diffraction peaks are observed

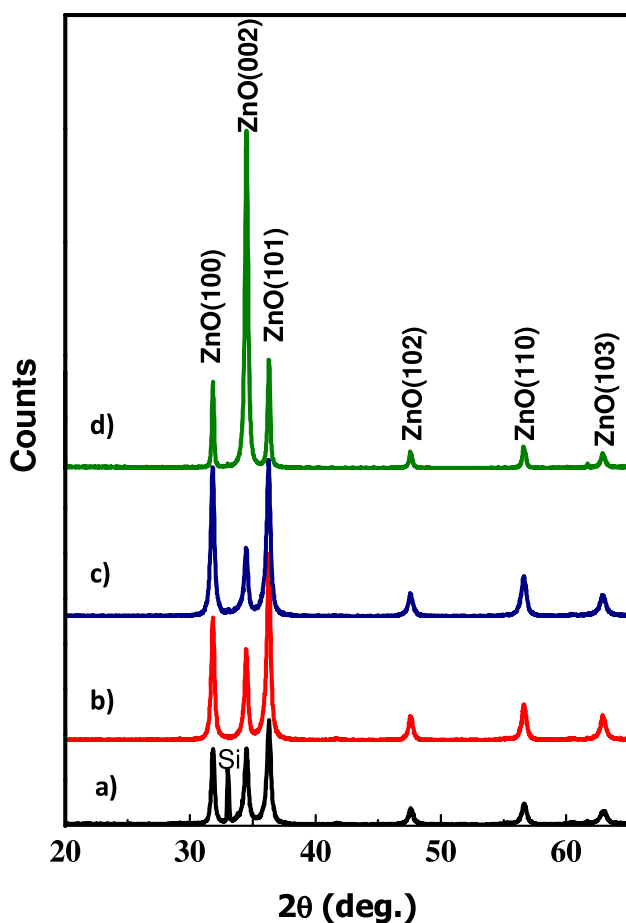


Fig. 1. XRD charts of ZnO deposited on bare Si substrate at (a) sample I: 0.15, (b) sample II: 0.30, (c) sample III: 0.70, and (d) sample IV: 1.00 Torr.

for metallic zinc, other phases, or any other impurities expect the Si peak observed at 33.5° due to the substrate. As the deposition pressure increased, the preferred orientation of crystallization changed from (1 0 1) to (0 0 2), keeping the hexagonal structure. The full width at half maximum value of the peaks decreased with increasing the deposition pressure, leading to an increase in the crystallite size. The effect of deposition pressure on the average crystallite size, D , is estimated by well-known Scherrer equation. The average crystallite size is slightly increased from ~ 3 to 6 nm when the deposition pressure increased from 0.15 to 1 Torr.

The morphology of ZnO nanostructures is shown in Fig. 2. It is observed that ZnO nanostructure was significantly affected by the variation of the deposition pressure. One may observe a considerable diversity in the geometrical parameters of 1D nanostructures. As observed in Fig. 2(a) of the sample I there are a kind of morphology with a smooth surface and high density; namely, one-side nanocombs. Each nanocomb

consists of several ZnO nanonails or nanoteeth parallel to each other. As seen in XRD charts of Fig. 1(a), the (1 0 1) intensity is slightly higher than (0 0 2) peak, indicating that ZnO has a preferred orientation along the (1 0 1) direction. The diameters of nanonails are irregular, where they are wide at the bottom and narrow at the tip. One-side nanocombs exhibit average diameter, length, and inter-distance between the nanonails of ~ 75 nm, $2 \mu\text{m}$, and $50\text{--}200$ nm, respectively. The morphology of the fabricated ZnO changed to a nanorods-like structure when the deposition pressure changed up to 0.3 Torr, as shown in Fig. 2(b). Each rod has an average length of $\sim 4 \mu\text{m}$ and diameter of ~ 400 nm. As the pressure was more increased up to 0.7 Torr, the nanorods-like structure increased in both length and diameter, as shown in Fig. 2(c). With increasing the pressure up to 1.0 Torr, a two-side nanocombs-like structure with thick and short teeth is formed. The growth of the teeth occurred in one and two opposite directions, as observed in Fig. 2(d).

The growth mechanism of ZnO nanostructures can be interpreted by the vapor–solid process, where no metal catalyst is used. The growth mechanism of the present method is illustrated in Fig. 3. First, the arrived atoms or molecules at the Si substrate adsorb on the surface (Fig. 3(a)). These adsorbed molecules react with each other as well as the substrate surface to form the bonds. The initial aggregation of the adsorbed species will be the nuclei of crystals (Fig. 3(b)). As a result of the vapor continuity, some of the small crystals were grown from limited nucleation sites to form 1D nanostructure (Fig. 3(c)). If the growth pressure is changed, the growth temperature is expected to change, leading to a change in the nucleation rate which causes a large change in the morphology of ZnO [28].

As it is clear from SEM images, the pressure is assumed to be an essential parameter for controlling the morphology of ZnO nanostructures. Liu et al. have reported on the fabrication of ZnO nanostructures via thermal evaporation at relatively high pressures and temperatures [26]. In their case, the geometrical dimensions (diameter or width) of the ZnO nanostructure were reduced as the deposition pressure increases. In the present method, the collisions between the atoms and ambient air lead to a reduction in the evaporation rate as compared with that at low pressure. However, if the pressure is high, the oxygen and the zinc partial pressure in the reaction chamber are high, and then the growth of as structure with a large dimension takes place. Thus, the geometrical dimensions are thinner for the thermal evaporation process performed at a low pressure. This observation

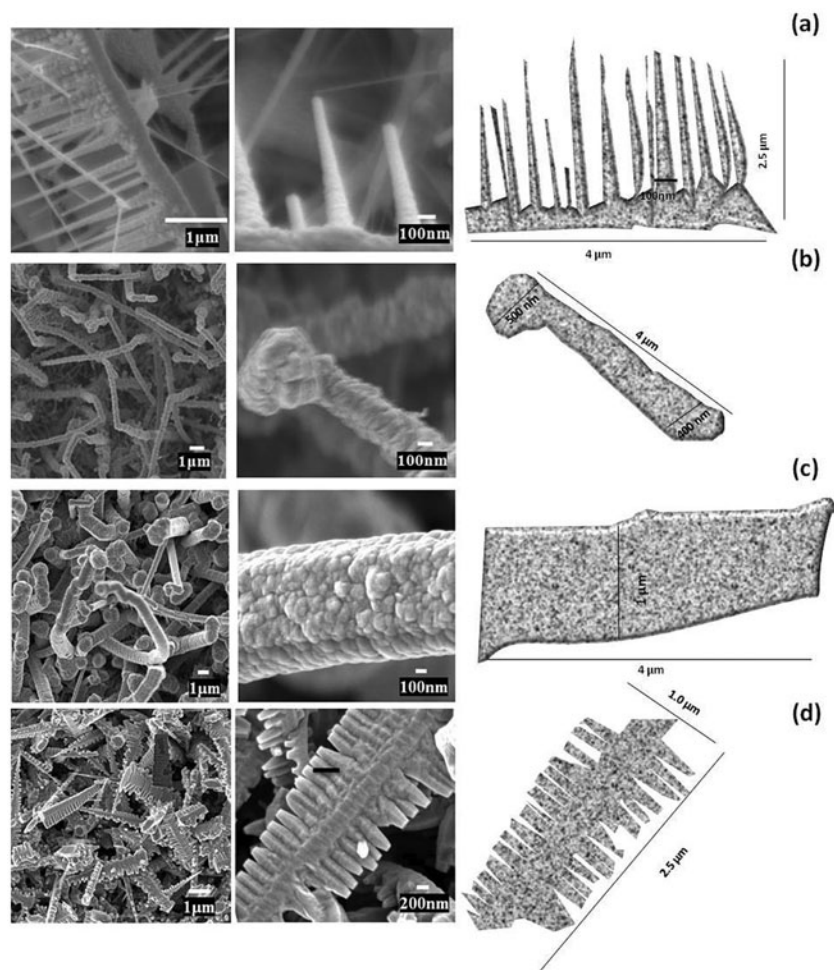


Fig. 2. Nanoscale geometry corresponding to FE-SEM images of the ZnO nanostructures grown by the thermal evaporation method for (a) 0.15, (b) 0.30, (c) 0.70, and (d) 1.00 Torr.

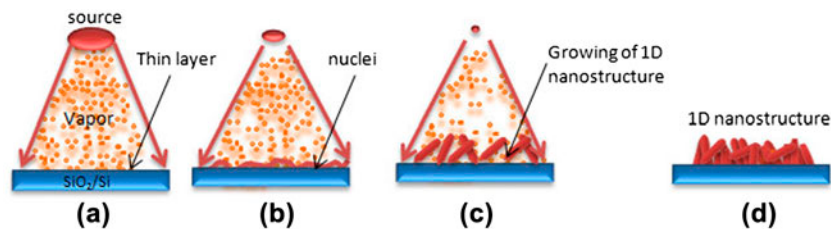


Fig. 3. Growth mechanism of 1D nanostructure: (a) arriving atoms or molecules at the Si substrate, (b) initial aggregation for formation of the nuclei, (c) starting growth of 1D nanostructure, and (d) the grown 1D nanostructure.

is a result of the nucleation rate which has a great impact on the nanostructure dimensions.

3.2. Photocatalytic activity of ZnO nanostructures

The photocatalytic activity of the fabricated ZnO nanostructures was evaluated by degradation of MB in water under UV light. Commonly, MB is a

representative organic dye in textile effluents, stable under visible light irradiation, and easily monitored by optical absorption spectroscopy [29]. The concentrations of MB during the photocatalytic reactions were determined by monitoring the changes of the main absorbance maximized at 664 nm.

Fig. 4 shows a selection of the absorbance variation of MB at different time intervals for the sample I, as

an example. It can be seen that water turned approximately colorless within 135 min of irradiation time. A similar experiment was carried out for other samples. The variation in concentration of MB solution is plotted with the irradiation time in Fig. 5. The degradation of MB with irradiation time can be described as an exponential function. As observed in Fig. 5, the sample I exhibited a significantly highest photocatalytic activity compared with the other samples. This observation exhibits a good correlation between the structural parameters of ZnO nanostructures and their photocatalytic activity. In a photocatalytic system, photo-induced molecular transformation or reaction takes place at the surface of the catalyst. A basic mechanism of photocatalytic reaction on the generation of an electron–hole pair and its destination is proposed as follows: when a photocatalyst is illuminated by energy higher than its band gap, electron migrates to the conduction band and hole is formed in the valence band. The holes can generate hydroxyl radicals which are highly oxidizing in nature. The holes could react with dye molecules and abstract electrons where the degradation process occurs [30–34].

The photo decolorization of MB in the presence UV light radiation is thought to be a pseudo-first-order kinetic reaction. The semi-logarithmic relationship of the concentration of MB vs. irradiation time yields a straight line, as shown in Fig. 6(a), indicating a pseudo-first-order reaction [35]. Using the following equation, one can calculate the degradation rate constant, k and the adsorption equilibrium constant, K [36]:

$$\ln\left(\frac{C}{C_0}\right) = -kKt + KC_0\left(1 - \frac{C}{C_0}\right) \quad (2)$$

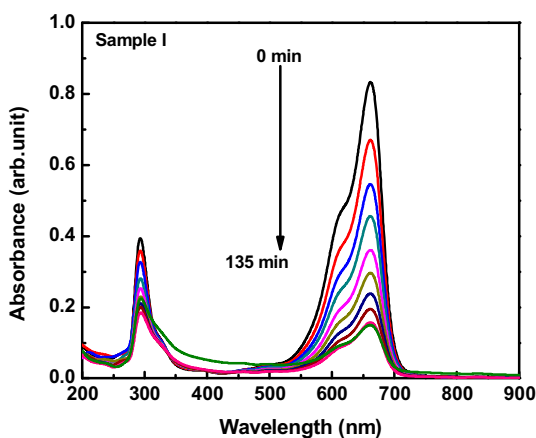


Fig. 4. Photocatalysis charts of ZnO deposited on Si substrate at 0.15 Torr, for an example.

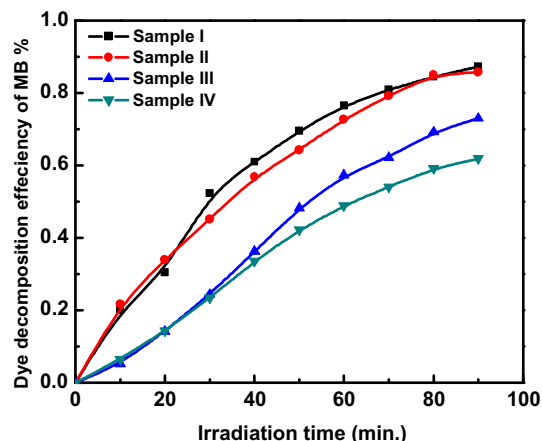


Fig. 5. Photocatalytic degradation of methylene blue (MB) on ZnO deposited on Si substrate deposited at different pressures.

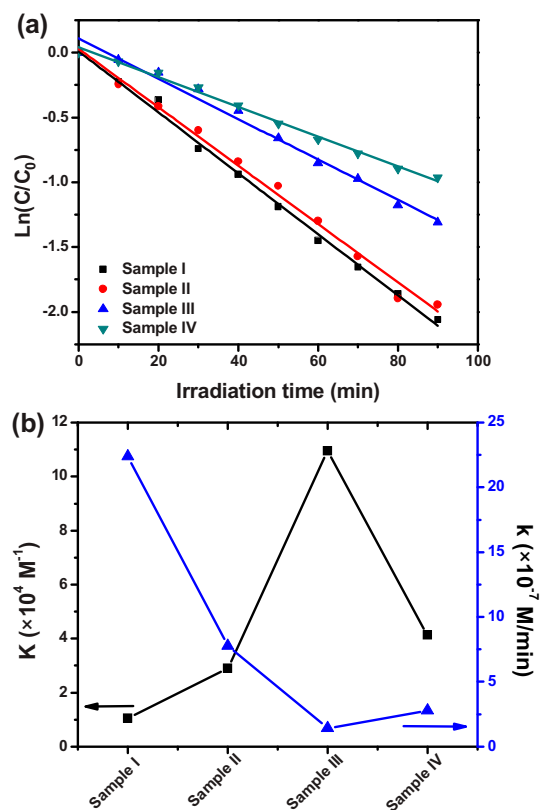


Fig. 6. (a) Semi-logarithmic graph of MB concentration vs. irradiation time in the presence of ZnO and (b) the dependence of the first-order reaction rate constants (k) and the adsorption equilibrium constant (K) of different structures.

when the concentration of MB is very low ($KC \ll 1$), the Eq. (2) can be simplified to the following Eq. (3):

$$\ln\left(\frac{C}{C_0}\right) = -kKt + KC_0 \quad (3)$$

Linear relation of $\ln(C/C_0)$ vs. the irradiation time, t , was obtained for every samples, as shown in Fig. 6(b). Accordingly, the values of K and k were estimated from the intercept and slope, respectively. As obvious from this figure, the sample I exhibits the faster reaction rate, while the sample III exhibits higher adsorption ability, comparing to the others. The MB maximum adsorption ability of $1.09 \times 10^5 \text{ M}^{-1}$ was observed for nanorod structure while the minimum adsorption ability of $1.05 \times 10^4 \text{ M}^{-1}$ was observed for one-side nanocombs structure. A contrary, the maximum degradation rate of $2.2 \times 10^{-6} \text{ M min}^{-1}$ was recorded for one-side nanocombs structure while the minimum degradation rate of $1.4 \times 10^{-7} \text{ M min}^{-1}$ was recorded for nanorod structure. The photocatalytic activity recorded for sample III is higher than that recorded for sample IV, although the lowest value of degradation rate of sample III. This could be attributed to the highest value of the adsorption equilibrium constant.

4. Conclusion

In summary, various morphologies of ZnO nanostructures such as one-, two-side nanocombs, and nanorods have been successfully synthesized by a developed thermal evaporation method. The morphology of ZnO was controlled by the variation of deposition pressure. XRD analysis studied the crystal structure and confirmed the pure phase of ZnO products prepared by the present method. The photocatalytic activity of these various morphologies was performed on methylene blue-wasted water. From the experimental observations, the photocatalytic activity of ZnO dramatically depends on the geometry of examined nanostructure. The degradation rate and the adsorption equilibrium constants were calculated for these different morphologies. It was found that one-side ZnO nanocombs of long nails exhibited much better photocatalytic efficiency comparing with other nanostructures.

Acknowledgment

The authors are thankful to Prof. Toshinari Yamazaki, University of Toyama, Japan for his support and valuable discussion.

References

- [1] Y. Li, F. Qian, J. Xiang, C.M. Lieber, Nanowire electronic and optoelectronic devices, *Mater. Today* 9 (2006) 18–27.
- [2] N.M. Shaalan, T. Yamazaki, T. Kikuta, Influence of morphology and structure geometry on NO_2 gas-sensing characteristics of SnO_2 nanostructures synthesized via a thermal evaporation method, *Sens. Actuators B* 153 (2011) 11–16.
- [3] Y. Shen, T. Yamazaki, Z. Liu, D. Meng, T. Kikuta, N. Nakatani, M. Saito, M. Mori, Microstructure and H_2 gas sensing properties of undoped and Pd-doped SnO_2 nanowires, *Sens. Actuators B* 135 (2009) 524–529.
- [4] M. Seol, E. Ramasamy, J. Lee, K. Yong, Highly efficient and durable quantum dot sensitized ZnO nanowire solar cell using noble-metal-free counter electrode, *J. Phys. Chem. C* 115(44) (2011) 22018–22024.
- [5] P. Pawinrat, O. Mekasuwandumrong, J. Panpranot, Synthesis of Au–ZnO and Pt–ZnO nanocomposites by one-step flame spray pyrolysis and its application for photocatalytic degradation of dyes, *Catal. Commun.* 10(10) (2009) 1380–1385.
- [6] J. Liqiang, W. Dejun, W. Baiqi, L. Shudan, X. Baifu, F. Honggang, S. Jiazhong, Effects of noble metal modification on surface oxygen composition, charge separation and photocatalytic activity of ZnO nanoparticles, *J. Mol. Catal. A Chem.* 244(1–2) (2006) 193–200.
- [7] Z.L. Wang, Nanostructures of zinc oxide, *Mater. Today* 7(6) (2004) 26–33.
- [8] R.M. Mohamed, M.A. Barakat, Enhancement of photocatalytic activity of ZnO/ SiO_2 by nanosized Pt for photocatalytic degradation of phenol in wastewater, *Int. J. Photoenergy* 2012 (2012) Article ID 103672, 8 p.
- [9] G. Broasca, G. Borcia, N. Dumitrascu, N. Vrinceanu, Characterization of ZnO coated polyester fabrics for UV protection, *Appl. Surf. Sci.* 279 (2013) 272–278.
- [10] X. Mo, G. Fang, H. Long, S. Li, H. Huang, H. Wang, Y. Liu, X. Meng, Y. Zhang, C. Pan, Near-ultraviolet light-emitting diodes realized from n-ZnO nanorod/p-GaN direct-bonding heterostructures, *J. Lumin.* 137 (2013) 116–120.
- [11] F. Jamali-Sheini, R. Yousefi, D.S. Joag, M.A. More, Influence of chemical routes on optical and field emission properties of Au–ZnO nanowire films, *Vacuum* 101 (2014) 233–237.
- [12] J. Xu, K. Fan, W. Shi, K. Li, T. Peng, Application of ZnO micro-flowers as scattering layer for ZnO-based dye-sensitized solar cells with enhanced conversion efficiency, *Sol. Energy* 101 (2014) 150–159.
- [13] Y. Abdi, S.M. Jebreil Khadem, P. Afzali, Resonantly excited ZnO nanowires for fabrication of high sensitivity gas sensor, *Curr. Appl. Phys.* 14 (2014) 227–231.
- [14] Z. Yin, S. Wu, X. Zhou, X. Huang, Q. Zhang, F. Boey, H. Zhang, Electrochemical deposition of ZnO nanorods on transparent reduced graphene oxide electrodes for hybrid solar cells, *Small* 6(2) (2010) 307–312.
- [15] V. Abramova, A. Sinitskii, Large-scale ZnO inverse opal films fabricated by a sol-gel technique, *Superlattices Microstruct.* 45(6) (2009) 624–629.
- [16] A. Mohanta, J.G. Simmons, H.O. Everitt, G. Shen, S.M. Kim, P. Kung, Effect of pressure and Al doping on structural and optical properties of ZnO nanowires

- synthesized by chemical vapor deposition, *J. Lumin.* 146 (2014) 470–474.
- [17] Y.J. Noh, S.I. Na, S.S. Kim, Inverted polymer solar cells including ZnO electron transport layer fabricated by facile spray pyrolysis, *Sol. Energy Mater. Sol. Cells* 117 (2013) 139–144.
- [18] G. Shen, Y. Bando, C.J. Lee, Synthesis and evolution of novel hollow ZnO urchins by a simple thermal evaporation process, *J. Phys. Chem. B* 109(21) (2005) 10578–10583.
- [19] E. Oh, H.Y. Choi, S.H. Jung, S. Cho, J.C. Kim, K.H. Lee, S.W. Kang, J. Kim, J.Y. Yun, S.H. Jeong, High-performance NO₂ gas sensor based on ZnO nanorod grown by ultrasonic irradiation, *Sens. Actuators B* 141 (1) (2009) 239–243.
- [20] J. Lee, K.N. Hui, K.S. Hui, Y.R. Cho, H.H. Chun, Low resistivity of Ni–Al co-doped ZnO thin films deposited by DC magnetron sputtering at low sputtering power, *Appl. Surf. Sci.* 293 (2014) 55–61.
- [21] J.Y. Kim, H. Jeong, D.J. Jang, Hydrothermal fabrication of well-ordered ZnO nanowire arrays on Zn foil: Room temperature ultraviolet nanolasers, *J. Nanopart. Res.* 13(12) (2011) 6699–6706.
- [22] F. Ye, A. Ohmori, C. Li, New approach to enhance the photocatalytic activity of plasma sprayed TiO₂ coatings using p-n junctions, *Surf. Coat. Technol.* 184(2–3) (2004) 233–238.
- [23] T. Tan, Y. Li, Y. Liu, B. Wang, X. Song, E. Li, H. Wang, H. Yan, Two-step preparation of Ag/tetrapod-like ZnO with photocatalytic activity by thermal evaporation and sputtering, *Mater. Chem. Phys.* 111(2–3) (2008) 305–308.
- [24] M.N. Chong, B. Jin, C.W. Chow, C. Saint, Recent developments in photocatalytic water treatment technology: A review, *Water Res.* 44(10) (2010) 2997–3027.
- [25] I. El Saliby, L. Erdei, J.H. Kim, H.K. Shon, Adsorption and photocatalytic degradation of methylene blue over hydrogen–titanate nanofibres produced by a peroxide method, *Water Res.* 47(12) (2013) 4115–4125.
- [26] W.-C. Liu, C.A.I. Wei, X.-L. Meng, Effects of temperature and pressure on morphologies of quasi-one-dimensional ZnO nanostructures fabricated via thermal evaporation, *Trans. Nonferrous Met. Soc. China* 16 (2006) s337–s340.
- [27] N.M. Shaalan, T. Yamazaki, T. Kikuta, Synthesis of metal and metal oxide nanostructures and their application for gas sensing, *Mater. Chem. Phys.* 127 (2011) 143–150.
- [28] B.M. Thaddeus, O. Hiroaki, P.R. Subramanian, K. Linda, *Binary Alloy Phase Diagrams*, Materials Park, Ohio, 1990.
- [29] M. Rashad, N.M. Shaalan, M.M. Hafiz, Enhanced photocatalytic of ZnO nanostructures via shape controlled platinum thin film, *Digest J. Nanomater. Biostructures* 10 (2015) 823–830.
- [30] N. Kislov, J. Lahiri, H. Verma, D.Y. Goswami, E. Stefanakos, M. Batzill, Photocatalytic degradation of methyl orange over single crystalline ZnO: Orientation dependence of photoactivity and photostability of ZnO, *Langmuir* 25(5) (2009) 3310–3315.
- [31] S. Baruah, M. Jaisai, R. Imani, M.M. Nazhad, J. Dutta, Photocatalytic paper using zinc oxide nanorods, *Sci. Technol. Adv. Mater.* 11(5) (2010) Article ID 055002, 7 p.
- [32] H. Zhu, R. Jiang, Y. Fu, Y. Guan, J. Yao, L. Xiao, G. Zeng, Effective photocatalytic decolorization of methyl orange utilizing TiO₂/ZnO/chitosan nanocomposite films under simulated solar irradiation, *Desalination* 286 (2012) 41–48.
- [33] M. Qamar, M. Muneer, A comparative photocatalytic activity of titanium dioxide and zinc oxide by investigating the degradation of vanillin, *Desalination* 249(2) (2009) 535–540.
- [34] M. Nirmala, M.G. Nair, K. Rekha, A. Anukaliani, S.K. Samdarshi, R.G. Nair, Photocatalytic activity of ZnO nanopowders synthesized by DC thermal plasma, *Afr. J. Basic Appl. Sci.* 2 (2010) 161–166.
- [35] M.A. Behnajady, N. Modirshahla, M. Shokri, B. Rad, Enhancement of photocatalytic activity of TiO₂ nanoparticles by silver doping: Photodeposition versus liquid impregnation methods, *Global Nest J.* 10(1) (2008) 1–7.
- [36] H. Yan, J. Hou, Z. Fu, B. Yang, P. Yang, K. Liu, M. Wen, Y. Chen, S. Fu, F. Li, Growth and photocatalytic properties of one-dimensional ZnO nanostructures prepared by thermal evaporation, *Mater. Res. Bull.* 44 (2009) 1954–1958.